JOURNAL OF GEOPHYSICAL RESEARCH, VOL. 115, C03018, doi:10.1029/2009JC005545, 2010

An assessment of surface heat fluxes from J-OFURO2 at the KEO and JKEO sites

Hiroyuki Tomita,[1] Masahisa Kubota,[2] Meghan F. Cronin,[3] Shinsuke Iwasaki,[2] Masanori Konda,[1] and Hiroshi Ichikawa[1]

Received 29 May 2009; revised 4 September 2009; accepted 2 October 2009; published 17 March 2010.

[1] The daily mean air-sea heat fluxes over the global oceans have been developed as the version 2 of Japanese Ocean Flux data sets with use of Remote sensing Observations (J-OFURO2). Net heat flux is available from 1988 to 2006, and the turbulent heat flux is available from 1988 to 2007. To assess the accuracy of the J-OFURO2 product over the Kuroshio Extension region, air-sea heat fluxes and related state variables were compared with independent in situ observations from the Kuroshio Extension Observatory (KEO) and JAMSTEC KEO (JKEO) surface moorings. Although seasonal biases were found, these tended to cancel out over the total period, resulting in a total bias and RMS in J-OFURO2 net heat fluxes of 8.6 and 56.8 W/m^2, respectively. Comparisons with other global air-sea heat flux products from numerical weather prediction, i.e., the National Centers for Environmental Prediction (NCEP)/National Center for Atmospheric Research (NCAR) reanalysis (NRA1), the NCEP/Department of Energy reanalysis (NRA2), and satellite observations, i.e., Hamburg Ocean Atmosphere Parameters and Fluxes from Satellite data and merged product, i.e., Objectively Analyzed Air-Sea Fluxes were also conducted at the KEO and JKEO sites. Comparison results show that the total and seasonal biases are smallest compared with other products, and J-OFURO2 air-sea heat fluxes are best data set for air-sea interaction study over the Kuroshio Extension region.

Citation: Tomita, H., M. Kubota, M. F. Cronin, S. Iwasaki, M. Konda, and H. Ichikawa (2010), An assessment of surface heat fluxes from J-OFURO2 at the KEO and JKEO sites, *J. Geophys. Res.*, *115*, C03018, doi:10.1029/2009JC005545.

1. Introduction

[2] Global air-sea heat flux data sets are required for many studies related to air-sea interaction, global climate change, and atmospheric and oceanic general circulations [*Curry et al.*, 2004]. Air-sea heat fluxes are typically computed by applying a bulk algorithm to a set of state variables that includes surface air and sea temperature, surface humidity, and surface wind relative to the ocean currents. Typically, ocean currents are assumed to be small relative to the winds are neglected, an assumption that can be questionable in regions of strong currents such as the Kuroshio Extension. Global data sets of these state variables are provided by the following: (1) voluntary observing ship (VOS) observations, (2) numerical weather prediction (NWP) analyses or reanalyses, (3) satellite observations, or (4) a combination of (1)–(3). The latter type, which uses a combination of data sources, is referred to as a hybrid product. While air-sea heat flux products based on the VOS fields provide long time series, they suffer from serious sampling error due to sparse observations. Likewise, flux products based on the NWP analyses or reanalyses are widely used by many researchers but can have serious errors as reported by several comparison studies with in situ observations [i.e., *Moore and Renfrew*, 2002; *Sun et al.*, 2003; *Qiu et al.*, 2004; *Kubota et al.*, 2008]. Satellite-based products have much higher spatial resolution compared to the VOS- and NWP-based flux products but can have large errors due to inaccuracies in the satellite-based humidity and air temperature state variables. For example, the Japanese Ocean Flux Data Sets with Use of Remote Sensing Observations (J-OFURO) [*Kubota et al.*, 2002] constructed in 2000 (J-OFURO1) had errors similar in magnitude to the NWP fluxes [*Tomita and Kubota*, 2006]. Recently, however, an updated version 2 J-OFURO of satellite-derived air-sea heat flux data set (J-OFURO2) has been constructed. In this study we use surface mooring observations from the Kuroshio Extension region to assess this new J-OFURO2 product.

[3] The Kuroshio and the Kuroshio/Oyashio Extension regions have some of the most intense air-sea interactions in the global ocean. In particular, the confluence of the Kuroshio/Oyashio currents in this region generates a strong sea surface temperature (SST) front that can project into the atmospheric boundary layer (ABL) and potentially to the top of the troposphere through the air-sea heat flux effects on the ABL stability and pressure gradients [*Tokinaga et al.*,

[1]Research Institute for Global Change, Japan Agency for Marine and Earth Science Technology, Yokosuka, Japan.
[2]School of Marine Science and Technology, Tokai University, Shizuoka, Japan.
[3]Pacific Marine Environmental Laboratory, NOAA, Seattle, Washington, USA.

0148-0227/10/2009JC005545

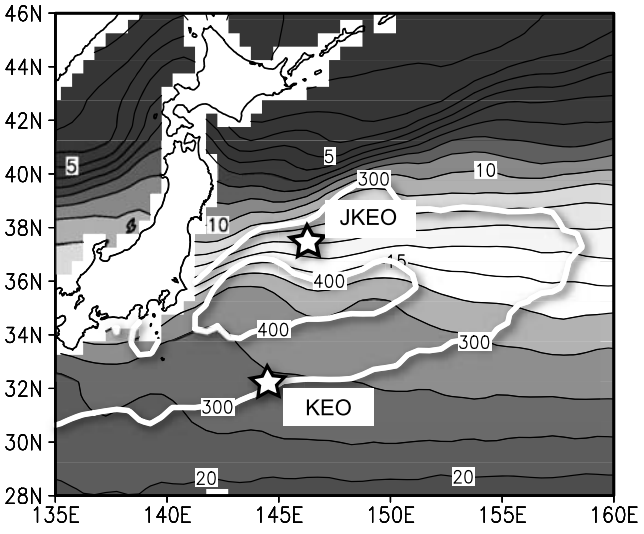

Figure 1. Locations of the KEO and JKEO buoys (stars) superimposed on the SST (filled) and the turbulent heat flux (white contours) derived from COADS wintertime climatology during 1960–1997. SST units are degree Celsius. Turbulent heat flux units are W/m^2.

2009; *Small et al.*, 2008; *Minobe et al.*, 2008]. During boreal winter, strong westerly winds and the intrusion of cold and dry air of continental origin, blowing over the warm waters of the Kuroshio and the Kuroshio/Oyashio Extension regions, lead to extremely large latent and sensible heat loss by the ocean (Figure 1). Thus, a comparison with observations in these regions provides a critical test of the product. While the extremely strong currents and heavy weather conditions make in situ observations difficult in these regions, in June 2004, the National Oceanic and Atmospheric Administration (NOAA) deployed the Kuroshio Extension Observatory (KEO) surface mooring in the Kuroshio Extension recirculation gyre as a contribution to the global network of OceanSITES time series reference stations. Furthermore, in February 2007, through a partnership between NOAA and the Japan Agency for Marine-Earth Science and Technology, a second surface mooring, referred to as JAMSTEC KEO (JKEO), was deployed north of the Kuroshio Extension jet (Figure 1). These buoys provide relatively long, continuous, high-quality air-sea heat flux time series in the Kuroshio Extension region that can be used as reference time series for assessing gridded global air-sea flux products.

[4] Using the KEO buoy data, *Kubota et al.* [2008] showed that biases in the air-sea heat fluxes obtained from the National Centers for Environmental Prediction (NCEP)/National Center for Atmospheric Research (NCAR) reanalysis version 1 (NRA1) [*Kalnay et al.*, 1996] and the NCEP/Department of Energy (DOE) reanalysis (NRA2) [*Kanamitsu et al.*, 2002] were larger than those found in the tropics [*Jiang et al.*, 2005; *Tomita and Kubota*, 2006]. Data from the JKEO buoy were not available for their analysis and the assessment did not extend to satellite-derived air-sea heat flux products. Therefore, an objective of the present study is to assess the new satellite-derived J-OFURO2 air-sea heat flux data using high-quality in situ data obtained from both the KEO and JKEO surface moorings in the Kuroshio Extension region. As a first step, errors in KEO and JKEO fluxes are evaluated. Sources of errors in the J-OFURO2 product are then identified, and the seasonal and regional biases are analyzed through a set of tests described in section 2.

2. Data and Method

2.1. J-OFURO2 Air-Sea Heat Flux Data Set

[5] As discussed in section 1, global latent and sensible heat fluxes (LHF and SHF) are generally estimated by a bulk method. In J-OFURO2, the LHF and SHF are calculated from state variables: Surface wind speed (WND), air-sea specific humidity difference (DQ, i.e., the saturated specific humidity at the sea surface temperature, QS minus surface air specific humidity, QA), and air-sea temperature difference (DT, i.e., the SST minus air temperature, TA). The largest changes in J-OFURO2 LHF and SHF from J-OFURO1 are in the estimation of these state variables. Although J-OFURO1 uses data from only a single Defense Meteorological Satellite Program (DMSP)/Special Sensor Microwave Imager (SSMI), J-OFURO2 uses multisatellite and sensors to determine WND, QA, and SST (QS). Merging data from multiple satellites can significantly improve spatial coverage and reduce sampling error of the daily mean value [*Tomita and Kubota*, 2010]. In particular, for J-OFURO2, WND is constructed from a combination of microwave radiometers, i.e., DMSP/SSMI F08, F10, F11, F13, F14, F15, Aqua/Advanced Microwave Scanning Radiometer–Earth observing system (Aqua/AMSR-E), Tropical Rainfall Measurement Mission (TRMM)/TRMM Microwave Imager (TMI), and microwave scatterometers (ERS/AMI and QuikSCAT/SeaWinds). On the other hand, only data from the DMSP/SSMIs sensors (i.e., F08, 10, 11, 13, and 14) are used for estimating QA in J-OFURO2. The retrieving algorithm for QA from DMSP/SSMIs is unchanged from J-OFURO1 and is based on the work of *Schlussel et al.* [1995]. In order to merge QA from different satellites/sensors, i.e., Aqua/AMSR-E and TRMM/TMI, retrieving algorithms are needed for each sensor. Such algorithms are presently under development [*Kubota and Hihara*, 2008]. Finally, for SST, J-OFURO2 uses the new merged multisatellite and in situ product MGDSST [*Kurihara et al.*, 2006] constructed by Japan Meteorological Agency (JMA) instead of the Reynolds SST [*Reynolds and Smith*, 1994] used in J-OFURO1. This change is based on the results of *Iwasaki et al.* [2008] intercomparison and evaluation of five kinds of global SST products and the fact that the new satellite microwave observations provide global SST in all weather condition [*Chelton and Wentz*, 2005]. In particular, MGDSST merges in situ and microwave observations by Aqua/AMSR-E in addition to advanced very high resolution radiometer (AVHRR) observations.

[6] Because of the difficulty of estimating TA over the sea from space, J-OFURO1 did not use a bulk method for calculation of SHF but instead used a Bowen ratio method [*Kubota and Mitsumori*, 1997]. The ratio of SHF to LHF (i.e., Bowen ratio) in J-OFURO1 was set as the climatological mean of Bowen ratios calculated from the European Centre for Medium Range Weather Forecasting (ECMWF) data. J-OFURO1 LHF, combined with the Bowen ratio, provided J-OFURO1 SHF data. On the other hand, J-OFURO2

calculates SHF using a bulk algorithm with TA data derived from reanalysis of NWP, NRA2.

[7] Daily means of the J-OFURO2 state variables WND, QA, TA, and SST are gridded on regular 0.25° and 1.0° grids over the ice-free global oceans (mainly 60°S–60°N). An optimum interpolation method (OIM) is used for gridding QA and SST, while WND is gridded by simply averaging the abundance of wind data from multiple satellites/sensors. J-OFURO2 LHF and SHF are then calculated from these daily mean state variables using a bulk method.

[8] Comparison studies of bulk formulae with direct measurements of surface fluxes from eddy correlation method reveal that the bulk method used in J-OFURO1 [i.e., *Kondo*, 1975] causes systematic error in estimation of LHF, whereas the COARE 3.0 bulk algorithm [*Fairall et al.*, 2003] was one of most reliable flux algorithms [*Brunke et al.*, 2003]. Therefore, the COARE 3.0 bulk algorithm is used in J-OFURO2 for estimation of SHF and LHF. It should be noted, however, that bulk SST, with no corrections for warm layer and cool skin effects, is used as the skin temperature in the J-OFURO2 flux calculation.

[9] Because the J-OFURO1 used only the Japanese Geostationary Satellite for estimating the radiation flux data, i.e., short-wave and long-wave radiation (SWR and LWR), these fields, and the J-OFURO1 net air-sea heat flux (NET) were limited to the region of the eastern Indian Ocean and the western and central Pacific Ocean between 60°N and 60°S, 80°E and 160°W. However, many studies call for global net air-sea heat flux data. Therefore, J-OFURO2 also provides global NET data estimated from the global turbulent heat flux data and from global surface net radiation flux data obtained from the International Satellite Cloud Climatology Project (ISCCP). In particular, net SWR and LWR are divided into their upward and downward components, i.e., USWR, ULWR, DSWR, and DLWR, where SWR = USWR − DSWR and LWR = ULWR − DLWR. ISCCP values are used for all radiation flux components except for ULWR. In order to maintain consistency with turbulent heat flux calculations, J-OFURO2 estimates the ULWR using MGDSST. Because ISCCP provides radiation flux data only through 2006, NET in J-OFURO2 is calculated through 2006.

[10] In this study, we assessed the daily mean J-OFURO2 air-sea heat flux data that is on the 1° grid. Daily and monthly means of J-OFURO2 LHF, SHF, and state variables from 1988 to 2007 (20 years) are available via the Internet (see the J-OFURO2 web site). Daily and monthly means of NET are available for 1988–2006 (19 years). A high-resolution 0.25° grid version of J-OFURO2 LHF and SHF are also public for recent years, from 2002 to 2006.

2.2. KEO and JKEO Buoy Data

[11] To assess the new J-OFURO2 air-sea heat flux product, we performed comparisons with independent in situ data obtained from the KEO and JKEO buoys [*Cronin et al.*, 2008]. The KEO and JKEO buoys were deployed in the Kuroshio Extension recirculation gyre at 144.6°E, 32.4°N (nominal) and north of the Kuroshio Extension front at 146.5°E, 38.0°N, respectively (see Figure 1). Both buoys monitor air-sea heat, moisture, momentum and carbon dioxide fluxes, and upper ocean temperature, salinity, and currents. The delayed-mode high-resolution data from KEO are available for the period from 16 June 2004 through 14 September 2008 and from JKEO for the period from 18 February 2007 through 4 September 2008.

[12] J-OFURO2 air-sea heat flux time series are shown in comparison to the KEO flux time series in Figure 2 and in comparison to the JKEO flux time series in Figure 3. Surface turbulent heat flux and net radiation flux from the buoy data are calculated using the method described by *Kubota et al.* [2008]. Daily means of LHF and SHF are calculated using the COARE 3.0 algorithm [*Fairall et al.*, 2003] with high-resolution (10 min sampled) meteorological and ocean surface data. Sensor height correction for all meteorological parameters and warm layer and cool skin temperature corrections for the observed bulk SST were applied in the algorithm. The algorithm requires the speed of the surface wind relative to the surface current. Because of the data gaps in the KEO and JKEO current meter data, following *Cronin et al.* [2006] and *Kubota et al.* [2008], we estimated the relative wind speed using the satellite-derived 15 m current data from the Ocean Surface Current Analyses-Real Time (OSCAR) [*Bonjean and Lagerloef*, 2002]. As was done for the ISCCP radiation, net SWR and LWR fluxes are divided into their upward and downward components, i.e., USWR, ULWR, DSWR, and DLWR, where SWR = USWR − DSWR and LWR = ULWR − DLWR. DSWR and DLWR are measured by the KEO and JKEO buoys. USWR was calculated by reducing the DSWR by a factor of α, the albedo at the ocean surface, set as the ISCCP climatological monthly mean value. ULWR was calculated as ($\varepsilon\sigma$ SST^4 + (1 − ε) DLWR), where σ is the Stefan–Boltzman constant and ε is the emissivity at the ocean surface, set as 0.984 following *Konda et al.* [1994].

[13] Following *Kubota et al.* [2008] as a first step toward assessing the J-OFURO2 fluxes, we must quantify the accuracy of the KEO and JKEO fluxes. Measurement errors shown in Tables 1 and 2 are based either upon a statistical analysis of precalibrations and postcalibrations of sensors used on ATLAS moorings in the tropics [*Freitag et al.*, 2001] or upon manufacturer specification (see http://www.pmel.noaa.gov/keo/). The LHF and SHF errors associated with these measurement errors are summarized in Table 1 for KEO and Table 2 for JKEO. Note that the KEO errors listed in Table 1 are very similar to those listed in Table 1 of *Kubota et al.* [2008], differing only because of the longer time series used in this study. Total error for 10 min LHF for KEO is estimated to be ∼16 W/m^2. The total error of LHF for JKEO is estimated to be ∼10 W/m^2. Assuming that the standard deviation portion of the errors in the state variables is random, the total errors can be reduced through time averaging. With this assumption, the total errors for daily-averaged LHF for KEO/JKEO are estimated to be ∼4 W/m^2. As shown in Tables 1 and 2, the total error of SHF is relatively small compared to that of LHF.

2.3. Other Global Products

[14] Although the primary focus of this study is to assess accuracy of J-OFURO2 air-sea heat flux, it is important to determine the performance of the J-OFURO2 relative to the other global data set. Therefore, in addition to the comparison of J-OFURO2 with in situ buoy observations, we also

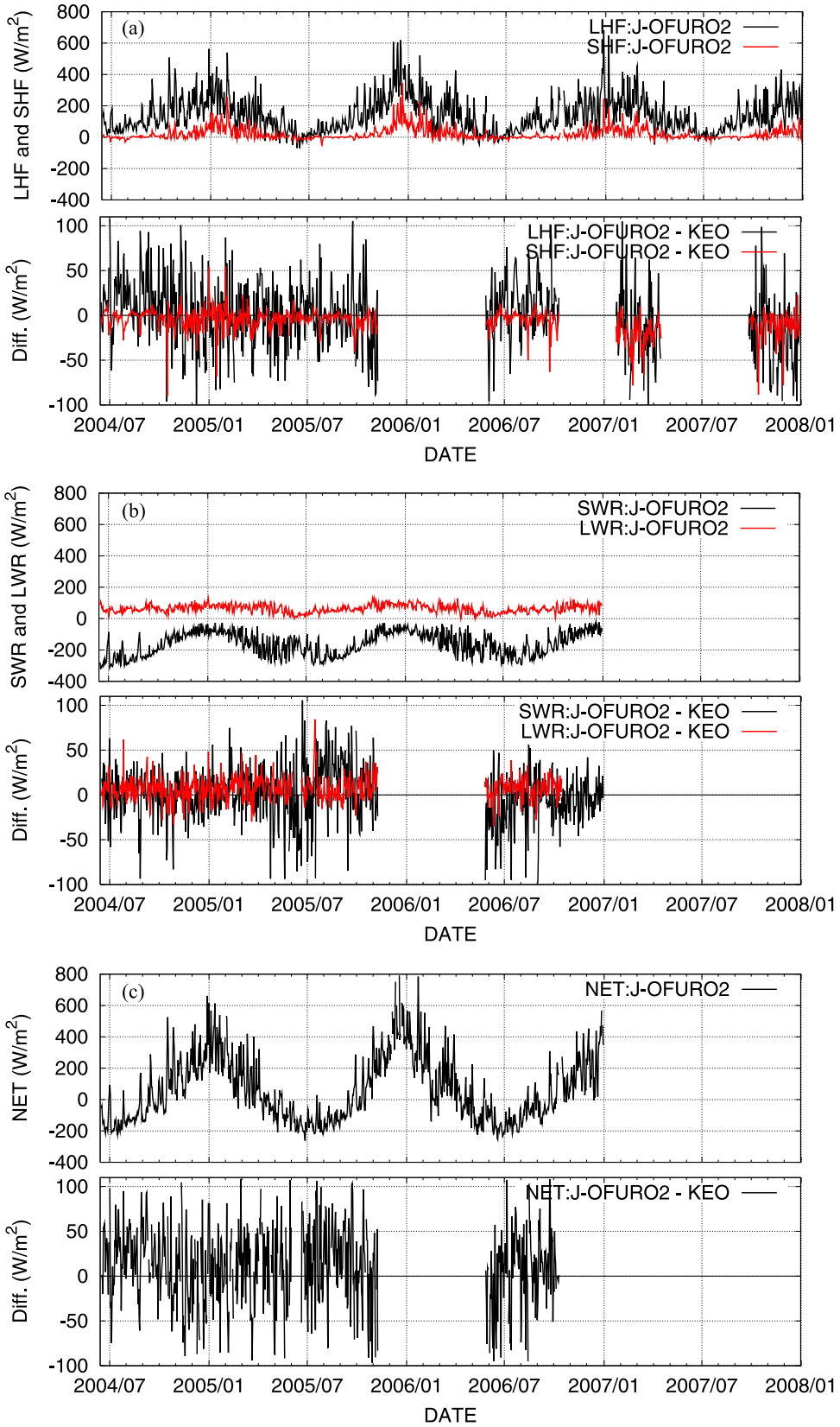

Figure 2. Daily mean time series of J-OFURO2 and J-OFURO2 minus KEO differences for (a) latent heat flux (LHF) (black) and sensible heat flux (SHF) (red), (b) net short-wave radiation (SWR) (black) and net long-wave radiation (LWR) (red), and (c) net heat flux, NET. A positive flux indicates an upward heat flux.

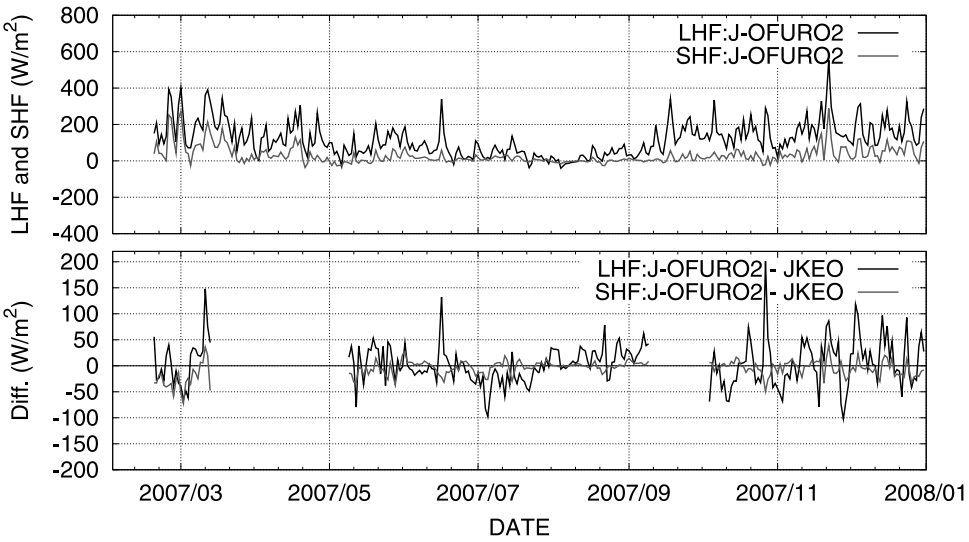

Figure 3. Same as Figure 2 but for LHF and SHF obtained from JKEO.

compared four different global air-sea heat flux products, including NRA1/2 and the Hamburg Ocean Atmosphere Parameters and Fluxes from Satellite data (HOAPS3), and a new hybrid product that synthesizes satellite and reanalysis products [OAFlux, *Yu and Weller*, 2007]. Although the NRA1/2 air-sea heat fluxes were assessed by *Kubota et al.* [2008] using the KEO buoy data, our study is the first comparison of the HOAPS3 and OAFlux products with moored reference data in the Kuroshio Extension region.

[15] Daily means of NRA1/2 surface air-sea heat fluxes are calculated from four times daily (i.e., 6 h average) data with T62 (about 210 km) spatial grids, following *Kubota et al.* [2008]. HOAPS3 provides twice daily air-sea heat flux data from 1987 to 2005 with 0.5° by 0.5° spatial grids. For HOAPS3, therefore, we calculated daily mean from the twice daily data. OAFlux provides daily mean of air-sea heat flux data from 1958 to 2006 with 1.0° by 1.0° spatial resolution. Note that HOAPS3 calculates LHF and SHF using the COARE 2.6 algorithm [*Fairall et al.*, 1996], a similar but slightly older version of the COARE 3.0 algorithm used in the buoy reference calculation, and the OAFlux and the J-OFURO2 flux calculations.

2.4. Comparison Strategy

[16] The comparison of J-OFURO2 (or other global products) with the KEO/JKEO data was conducted using daily mean data. To obtain J-OFURO2 (and other global products) value at the buoy positions, we linearly interpolated the fields to the buoy positions using the surrounding four grids values. Because the moorings were slack-line and had a watch circle diameter of ~10 km, and because the KEO anchor position changed slightly in several of the deployments, the position of the buoys for certain purposes should be considered variable. A rough estimate of the effect of the daily changes in the position of the KEO buoy on RMS error appeared to be small (within 1 W/m^2). Therefore to simplify the comparison, we used the nominal buoy positions to obtain the corresponding time series from the global products. The comparison results between the KEO/JKEO and J-OFURO2 air-sea heat flux and flux-related state variables are shown as basic statistics, i.e., a mean bias (J-OFURO2 − buoy), root mean square (RMS) of the differences, and a correlation coefficient. It should be noted that an air-sea heat flux from the ocean to the atmosphere (i.e., upward air-sea heat flux) is defined to have a positive sign in this study. Hence, a positive (negative) bias

Table 1. KEO Measurement Errors for Surface Wind Speed, Sea Surface Temperature, Air Temperature, and Relative Humidity and the Associated RMS and Bias Errors in Latent and Sensible Heat Flux[a]

	WND	SST	TA	RH	All	All (Daily Mean)
Assumed error						
RMS	±0.135 m/s	±0.018°C	±0.2°C	±2.7%	–	–
Random	±0.135 m/s	±0.0153°C	±0.198°C	±2.49%	–	–
Bias	0 m/s	0.0095°C	0.025°C	1.04%	–	–
LHF (W/m^2)						
RMS	2.1	0.6	5.8	13.8	15.2	3.3
Bias	0.0	0.3	−0.7	−5.1	−5.5	−3.5
SHF (W/m^2)						
RMS	0.4	0.2	2.8	0.2	2.8	0.2
Bias	0.0	0.1	−0.3	0.1	−0.1	−0.1

[a]"All" represents the total error for the 10 min latent heat flux (LHF) and sensible heat flux (SHF); "all (daily mean)" assumes that a portion of the measurement error is random and can be reduced when averaged over a day. WND, surface wind speed; SST, sea surface temperature; TA, air temperature; RH, relative humidity; RMS, root-mean-square.

Table 2. Same as Table 1 but for JKEO

	WND	TS	TA	RH	All	All (Daily Mean)
Assumed error						
RMS	±0.135 m/s	±0.018°C	±0.2°C	±2.7%	–	–
Random	±0.135 m/s	±0.0153°C	±0.198°C	±2.49%	–	–
Bias	0 m/s	0.0095°C	0.025°C	1.04%	–	–
LHF (W/m^2)						
RMS	1.4	0.4	3.7	8.6	9.5	2.1
Bias	0.0	0.2	−0.4	−2.7	−2.9	−2.7
SHF (W/m^2)						
RMS	0.5	0.2	2.6	0.1	2.6	0.3
Bias	0.0	0.1	−0.2	0.0	−0.1	−0.1

in the air-sea heat flux means that J-OFURO2 overestimates (underestimates) the upward air-sea heat flux compared with buoy, and an ocean model forced by this product would presumably be too cold (warm).

[17] *Kubota et al.* [2008] showed that errors in the reanalyses had a large seasonal dependence. For example, during winter, when prevailing winds were northerly and of continental origin, the reanalyses' humidity was too large; while during summer, when prevailing winds were southerly and of maritime origin, the humidity was too low. As a consequence, heat flux in this region had a large RMS error. Thus, in addition to the overall mean bias, RMS errors, and correlations, we also calculate biases during boreal winter and summer seasons corresponding to December, January, and February (DJF) and June, July, and August (JJA).

[18] In order to determine our best estimate of the errors, as well as the seasonal and regional dependence of these errors, we perform five different comparisons, referred to as comparisons 1–5 (see Table 3). In the following, we describe each comparison and its focus.

[19] In comparison 1, the KEO buoy data are compared with J-OFURO2 turbulent heat fluxes and its components. This comparison reveals differences in the turbulent heat fluxes between J-OFURO2 and KEO and possible reasons for these differences. The period of the comparison extends from 16 June 2004 to 31 December 2007, with several gaps due to trouble with the KEO mooring and sensors. These data gaps include periods from 10 November 2005 to 25 May 2006, from 16 October 2006 to 23 January 2007, and from 18 April 2007 to 26 September 2007. In total, 830 daily mean data are used in this comparison.

[20] Comparison 2 has a similar concept to comparison 1, but uses the JKEO buoy that was deployed north of the Kuroshio Extension front (see Figure 1). Since the JKEO observations start on 18 February 2007, this JKEO/J-OFURO2 comparison period is limited to 18 February 2007 to 31 December 2007. Also, because of some troubles with the JKEO sensors and electronics, data over the periods from 14 March 2007 to 8 May 2007 and from 10 September 2007 to 3 October 2007 are missing. As a result, 237 daily mean data are used in this comparison.

[21] To remove any interannual variations that could result in differences in the KEO and JKEO comparisons, comparison 3 is conducted during the period that has simultaneous observations at KEO and JKEO (i.e., from 18 February 2007 to 31 December 2007). It should be noted that the period of this comparison is quite a bit shorter than the other comparisons (113 days in total).

[22] While comparisons 1–3 focus on LHF and SHF, comparison 4 focuses on radiation and net heat fluxes (i.e., all surface heat fluxes) in addition to the turbulent heat fluxes. Since the J-OFURO2 provides net heat flux data only through 2006 due to the availability of ISCCP radiation data, we could not conduct the comparison using JKEO data. Therefore, comparison 4 was conducted only at the KEO buoy.

[23] Finally, comparison 5 compares the KEO LHF and SHF with five different global products, including J-OFURO2, HOAPS3, NRA1, NRA2, and OAFlux. The common period for this comparison is limited to 16 June 2004 to 9 November 2005.

2.5. Preestimated Error in J-OFURO2

[24] Because the bulk flux algorithm depends upon state variables, some errors in the J-OFURO2 fluxes can be predetermined. Similar to the propagation of error analyses for KEO and JKEO shown in Tables 1 and 2, a propagation of errors in the J-OFURO2 can be computed to determine a "preestimate" of the LHF and SHF errors for J-OFURO. These estimations of errors in J-OFURO2 are described in sections 2.5.1–2.5.5.

2.5.1. Eskin: Error Caused by Using Bulk SST Instead of Skin Temperature

[25] For proper estimation of surface heat flux, skin temperature data are required instead of bulk SST data. For the flux calculation with buoy data, we extrapolate the

Table 3. Summary of Comparisons

Name of Comparison	Brief Description	Period	Number of Comparison Daily Mean Data
Comparison 1	LHF SHF, longest time series at the KEO	Jun 2004 to Dec 2007	830
Comparison 2	LHF and SHF, longest time series at the JKEO	Feb 2007 to Dec 2007	237
Comparison 3	LHF and SHF, the time series of simultaneous observations for the KEO and JKEO	Feb 2007 to Dec 2007	113
Comparison 4	All Fluxes, longest time series at the KEO	Jun 2004 to Oct 2006	633
Comparison 5	Intercomparison with other global products at the KEO	Jun 2004 to Nov 2005	511

Table 4. Preestimated Errors in J-OFURO2 Turbulent Heat Fluxes[a]

	Eskin	Erw	Edm	Ets	Total
LHF (W/m^2)					
RMS	4.8	2.5	5.7	13.5	15.6
Bias	7.6	0.6	0.9	−0.1	9.1
SHF (W/m^2)					
RMS	2.0	0.5	2.1	2.7	4.0
Bias	2.8	0.1	0.0	−0.1	2.9

[a]Eskin is the error caused by using bulk SST instead of skin temperature. Erw is the error caused by using conventional wind instead of relative wind. Edm is error caused by using daily mean data for state variables in flux calculation. Ets is error caused by insufficient temporal sampling in the satellite measurements.

bulk 1 m SST to the surface using the model provided by the COARE 3.0 algorithm. J-OFURO2, however, uses bulk SST with no skin temperature correction for calculation of surface flux, since there are no appropriate skin temperature data for the global oceans and the extrapolation model requires subdiurnal flux estimates. Therefore, the difference between J-OFURO2 and buoy fluxes includes the error caused by using bulk SST instead of skin temperature, Eskin. We estimated Eskin by subtracting the flux calculated using the COARE 3.0 algorithm with the skin temperature correction from the flux calculated using the bulk temperature without the correction. Both flux estimates were based upon the same buoy data.

2.5.2. Erw: Error Caused by Using True Wind Speed Instead of Relative Wind Speed

[26] As discussed by *Fairall et al.* [2003], the surface flux estimation depends upon the speed of the surface wind relative to the sea surface current, instead of conventional surface wind speed. As mentioned in section 2.2, for flux calculations using buoy data, we estimated surface wind speed relative to the surface current using the satellite-derived 15 m current data from the OSCAR. On the other hand, for J-OFURO2 satellite-derived flux, the OSCAR current data were not used in the calculations in turbulent heat flux. *Kelly et al.* [2001] have indicated that satellite scatterometer measures wind speed relative to the ocean current rather than surface wind speed alone. The satellite scatterometers QuikSCAT and ERS are used in estimation of surface wind speed in J-OFURO2. However, the J-OFURO2 also uses microwave radiometer (e.g., SSM/I, AMSR-E, etc.) wind speed for better spatial temporal coverage and resolution. Accordingly, the J-OFURO2 surface wind speed data are a combined product of relative wind speed obtained from scatterometers and conventional winds obtained from radiometers. In order to know the potential impact on the flux calculation of using conventional wind speed rather than relative wind speed, we estimated Erw by subtracting the flux calculated using wind speed relative to the sea surface current obtained from OSCAR from the flux calculated using the conventional surface wind speed using the buoy data.

2.5.3. Edm: Difference Caused by Using or Not Using Daily Mean Data for Flux Calculation

[27] In general, most bulk flux algorithms require input state variables averaged over several minutes. For flux calculations using buoy data, we use state variables every 10 min or 2 min averages once per 10 min. On the other hand, J-OFURO2 uses daily mean state variables for the flux calculation because it is not feasible to obtain simultaneous observation of each state variable from various satellites more frequently than this. Therefore, the difference between J-OFURO2 and buoy fluxes includes the error caused by using daily mean state variables in J-OFURO2, Edm. Using the buoy data, we estimate Edm by subtracting the daily flux obtained from 10 min state variables from the flux obtained from daily mean state variables.

2.5.4. Ets and Ess: Difference Caused by Insufficient Temporal Sampling by Satellite Observation

[28] Most of the satellite data for WND, QA, and SST used in J-OFURO2 are obtained from Sun-synchronous satellites. That is, one satellite may observe surface parameters once or twice per day at the buoy location. Although multisatellite data are used to obtain daily mean to avoid adverse effect from such temporal sampling error, the sampling error might still remain. *Tomita and Kubota* [2010] demonstrated using buoy data that this type of temporal sampling error can have a large impact on accurate estimation of LHF. In this study, we estimate the temporal sampling error, Ets, for each state variable (i.e., WND, QA, and SST) using the KEO and JKEO buoy data following *Tomita and Kubota* [2010]. In addition, there could be an error caused by insufficient spatial sampling, Ess. It is difficult to estimate Ess using in situ observations. However, since the J-OFURO2 satellite fields have high spatial resolution, we assume that the Ess is adequately small compared to Ets.

2.5.5. Preestimated Errors in J-OFURO2 LHF and SHF

[29] Table 4 lists the estimated J-OFURO2 LHF and SHF errors associated with each of these factors (i.e., Eskin, Erw, Edm, and Ets) and the net error, assuming that each is independent. In particular, a net bias is estimated as the sum of each estimated bias, and a net RMS is estimated as the root of the sum of the square of the RMS for each factor, including the Ets for each state variable (the net Ets is listed in Table 4). The net biases for LHF and SHF are estimated to be 9.1 and 2.9 W/m^2, respectively. The largest estimated LHF bias error (7.6 W/m^2 in the daily mean) is caused by Eskin and is due to the cool skin effect rather than warm layer effect in COARE 3.0 (not shown here). The other bias errors are quite small (<1 W/m^2).

[30] The net RMS errors for LHF and SHF are estimated to be 15.6 and 4.0 W/m^2, respectively. The estimated RMS for Ets is 13.5 W/m^2 for LHF and has the largest impact on the net error. Other RMS errors are estimated to be ~6 W/m^2 and have relatively small impact on the net error. The largest components of Ets in LHF are those due to the unresolved temporal variability in WND (11.3 W/m^2) and QA (10.0 W/m^2).

3. Comparison Results

3.1. Comparisons 1 and 2: LHF and SHF at the KEO and JKEO Buoys

[31] Figure 2a shows the daily mean time series of LHF and SHF observed by the KEO buoy, with positive values indicating a heat transfer from the ocean to the atmosphere. LHF is characterized by a very large seasonal cycle with

Table 5. Comparison 1 Results for J-OFURO2 and KEO Buoy[a]

	All			Winter (DJF)			Summer (JJA)		
	Bias	RMS	Correlation	Bias	RMS	Correlation	Bias	RMS	Correlation
LHF	−0.9	43.6	0.92	−9.6	48.9	0.86	9.7	31.3	0.80
SHF	−6.7	13.1	0.92	−8.5	17.6	0.91	−2.7	7.7	0.64
WND	0.18	1.25	0.93	1.07	1.31	0.91	−0.25	1.15	0.91
QA	0.54	1.58	0.96	1.50	1.14	0.80	−0.28	1.38	0.82
QS	−0.05	0.52	0.99	0.08	0.28	0.98	−0.19	0.64	0.97
TA	0.85	0.94	0.99	1.53	0.78	0.96	0.24	0.70	0.94
SST	−0.01	0.45	0.99	0.06	0.34	0.97	−0.15	0.55	0.97
DQ	−0.60	1.58	0.86	−1.43	1.15	0.79	0.09	1.46	0.80
DT	−0.88	0.90	0.92	−1.45	0.82	0.92	−0.39	0.72	0.65

[a]See Table 3. Mean bias (J-OFURO2 − buoy) and RMS of bias for latent (LHF) and sensible (SHF) heat fluxes have units of W/m^2. Units are m/s for wind speed (WND). Units are g/kg for surface air specific humidity (QA), saturated specific humidity at the sea surface temperature (QS), and their difference, i.e., QS − QA (DQ). Units are °C for surface air temperature (TA), sea surface temperature (SST), and their difference, i.e., TS − TA (DT). JJA, June, July, and August; DJF, December, January, and February.

large heat fluxes in winter and small fluxes in summer. Table 5 and Figure 4 show statistics and scatter diagrams for the LHF and SHF comparisons between the KEO and J-OFURO2. Although a few days have extremely large differences between the buoy and J-OFURO LHF (>100 W/m^2), most of the data agree well with each other. Overall biases for LHF and SHF are −0.9 and −6.7 W/m^2. The bias of LHF is quite small and within the accuracy of daily mean of LHF obtained by the KEO buoy estimated in section 2.

[32] Relatively large biases, however, are found in winter and summer. The LHF biases in winter and summer are −9.6 and 9.7 W/m^2, respectively. These winter and summer biases thus tend to cancel and produce an extremely small bias when averaged over a full year. Similar cancellation of seasonal bias is found in the state variables, especially WND and QA (Figure 5 and Table 5). J-OFURO2 tends to overestimate WND and QA in winter at the KEO, and underestimate WND and QA in summer. The RMS errors in the LHF and SHF are also larger during winter than summer and are probably related to the larger fluxes during winter.

[33] The cause of the bias in LHF appears to be different in winter and summer. In winter, J-OFURO2 underestimates LHF due to underestimation of DQ (overestimation of QA). Meanwhile J-OFURO2 WND is overestimated in winter and tends to reduce the underestimation of LHF due to underestimating of DQ. In contrast to winter, in summer, J-OFURO2 overestimates LHF by about 10 W/m^2 due to overestimation of DQ. J-OFURO2 WND is barely underestimated in summer. Although the statistics show a very small mean bias for DQ (0.09 g/kg) in Table 5, this is a result of cancellation of errors over the course of each year.

[34] Table 6 shows the bias in JJA for each year. Positive biases in J-OFURO2 LHF are found in each year during JJA, and the largest bias is found in 2004. The biases in J-OFURO2 WND are negative, i.e., underestimation of 0.2–0.3 m/s in each year. On the other hand, biases in J-OFURO2 DQ show significant difference between each year. In 2004 and 2006, J-OFURO2 DQ is overestimated due to underestimation of QA. In contrast, in 2005, J-OFURO2 DQ is underestimated due to underestimation of QS.

[35] Table 7 shows comparison 2 statistics (i.e., comparison with the JKEO buoy). Figure 3 shows daily mean time series of LHF and SHF at JKEO. Also, Figure 6 shows time series of the flux-related parameters and the difference between JKEO and J-OFURO2. The JKEO buoy is located on the cold side of the Kuroshio Extension front, while the KEO buoy is located on the warm side of the front. Mean features of the turbulent heat flux and the related atmospheric and oceanic conditions are quite different at JKEO. For example, LHF at JKEO is smaller than that at KEO. On

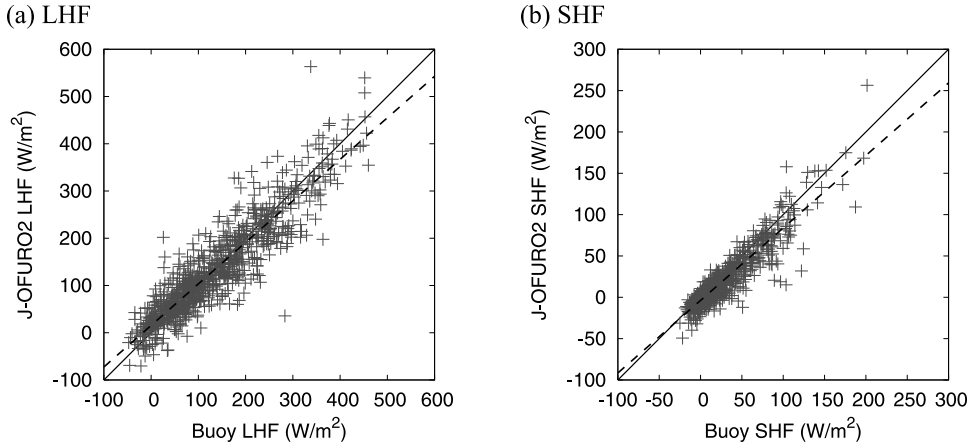

Figure 4. Scatter-diagrams of (a) LHF and (b) SHF from the KEO buoy and J-OFURO2. The linear regression line is shown as a dashed line. Note that the range is the difference between Figures 4a and 4b.

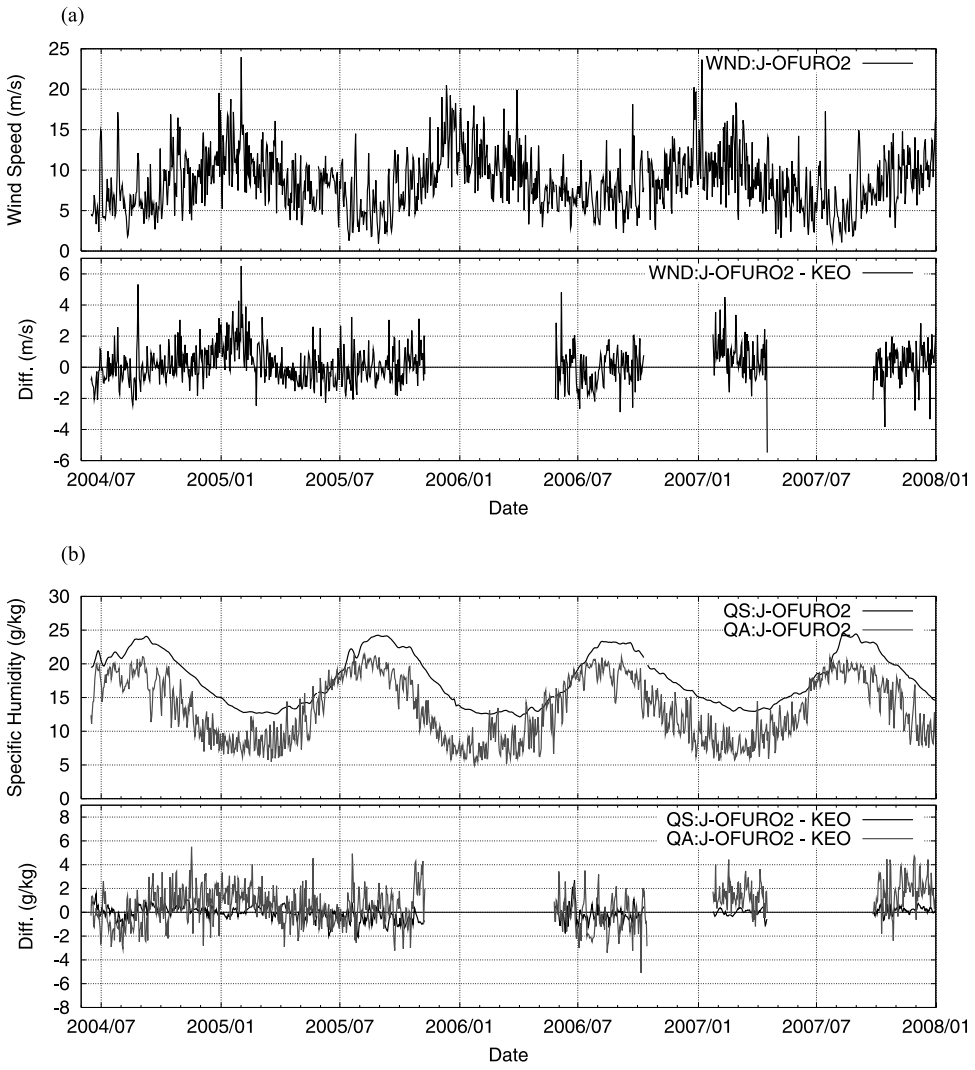

Figure 5. Time series of J-OFURO2 daily mean and the J-OFURO2 minus KEO difference for (a) wind speed (WND) and (b) saturated specific humidity at surface (QS) and surface air specific humidity (QA).

the other hand, SHF at JKEO is larger than that at KEO. Therefore, the accuracy of J-OFURO2 might be different at JKEO from that at KEO. The overall biases in LHF and SHF are small, 4.0 and −5.5, respectively. Seasonal biases are also found, and the bias and RMS in winter are larger than those in summer. These characteristics are similar to the results at KEO, although the sign of the bias in LHF is opposite at the two sites. Although J-OFURO2 LHF at KEO is underestimated (overestimated) in winter (summer), it is overestimated (underestimated) at JKEO. Overestimation of LHF in winter is due to overestimation of WND with a bias of 1.3 m/s. Meanwhile DQ is underestimated and mainly due to overestimation of QA. It is interesting that although the sign of the bias in LHF is different between KEO and JKEO, the sign of bias in WND and DQ is the same at both buoys.

3.2. Comparison 3: Comparison of the KEO and JKEO

[36] To investigate these differences between the KEO and JKEO comparisons, we performed comparison 3, using data from the period which has simultaneous observations at KEO and JKEO. Table 8 shows statistics for comparison 3. Note that the data used in this comparison are limited (113 days), and most of the data are centered in the period from October to December 2007.

[37] Although there are not large differences in RMS and correlation between turbulent heat fluxes at the KEO and JKEO, a significant difference is found in their biases over this common period. J-OFURO2 LHF and SHF at KEO have relatively large biases compared to the biases at JKEO. The biases in the J-OFURO2 LHF and SHF at KEO are −28.1 and −15.5 W/m^2, respectively. In contrast, the bias

Table 6. Biases for JJA for Each Year[a]

	2004	2005	2006	Total
LHF	20.0	2.1	8.7	9.7
WND	−0.3	−0.2	−0.2	−0.3
DQ	0.7	−0.5	0.2	0.1
QA	−0.7	0.1	−0.3	−0.3
QS	0.0	−0.4	−0.2	−0.2

[a]The units and abbreviations of variable are the same as Table 5.

Table 7. Comparison 2 Results for J-OFURO2 and JKEO Buoy[a]

	All			Winter (DJF)			Summer (JJA)		
	Bias	RMS	Correlation	Bias	RMS	Correlation	Bias	RMS	Correlation
LHF	4.0	41.2	0.90	15.4	42.2	0.87	−2.4	31.7	0.80
SHF	−5.5	15.6	0.96	−13.7	17.5	0.96	−1.7	9.8	0.80
WND	0.42	1.41	0.94	1.26	1.55	0.96	−0.17	0.88	0.95
QA	0.37	1.41	0.96	0.42	0.83	0.82	0.19	1.22	0.95
QS	−0.25	0.63	0.98	−0.19	0.57	0.74	−0.19	0.83	0.91
TA	0.64	1.18	0.99	1.73	0.71	0.97	0.06	1.19	0.93
SST	−0.23	0.79	0.98	−0.31	0.91	0.75	−0.21	0.81	0.91
DQ	−0.61	1.54	0.83	−0.62	1.04	0.68	−0.39	1.52	0.78
DT	−0.95	1.22	0.92	−2.04	1.15	0.90	−0.28	0.99	0.82

[a]See Tables 3 and 5.

in J-OFURO2 LHF at JKEO is positive, 6.0 W/m^2, and the bias in SHF is −8.6 W/m^2. The reason for the smaller biases at JKEO does not appear to be the differences in mean turbulent heat flux. For example, the mean LHF at KEO is about 40% larger than that at JKEO (see Figures 2 and 3). However, the difference in bias in LHF between the KEO and JKEO is greater than 400%. Therefore, the difference is likely due to differences in the flux-related parameter biases between the two sites. Table 8 indicates that the major source of the LHF bias is QA. The bias in QA at KEO and JKEO are 1.75 and 0.85 g/kg, respectively. These overestimations of QA in J-OFURO2 cause underestimation of

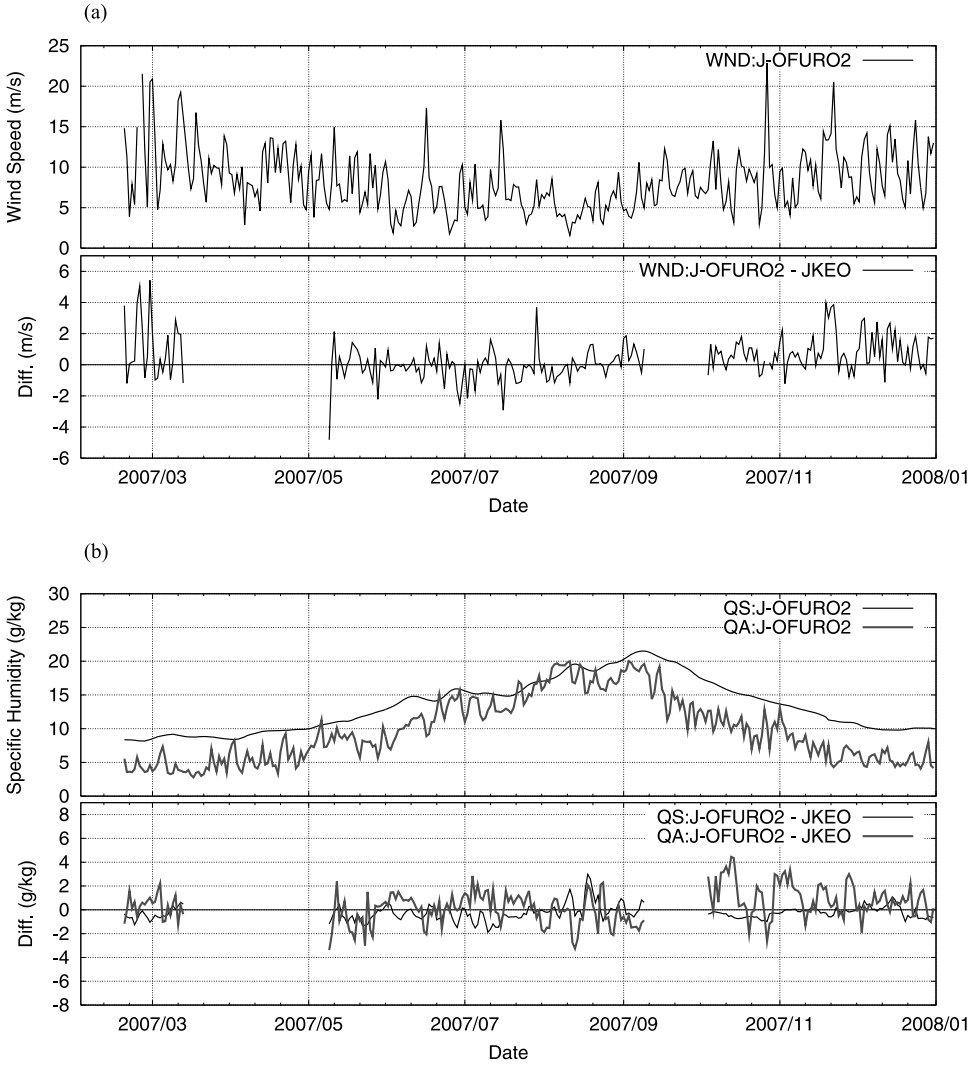

Figure 6. Daily mean time series of J-OFURO2 and the J-OFURO2 minus JKEO difference for (a) wind speed (WND) and (b) saturated specific humidity at surface (QS) and surface air specific humidity (QA).

Table 8. Comparison 3 Results for the Common Period Between J-OFURO2 and KEO/JKEO Buoys[a]

	Bias		RMS		Corr	
	KEO	JKEO	KEO	JKEO	KEO	JKEO
LHF	−28.1	6.0	52.4	49.3	0.86	0.84
SHF	−15.5	−8.6	17.6	18.8	0.90	0.95
WND	0.43	0.98	1.30	1.57	0.91	0.94
QA	1.75	0.85	1.34	1.37	0.94	0.86
QS	0.16	−0.25	0.29	0.44	1.00	0.99
TA	1.66	1.27	0.75	0.83	0.99	0.99
SST	0.15	−0.32	0.27	0.66	1.00	0.98
DQ	−1.59	−1.10	1.31	1.46	0.82	0.63
DT	−1.51	−1.59	0.86	1.04	0.91	0.92

[a]See Tables 3 and 5.

DQ and LHF. In addition, the biases in WND at KEO and JKEO are 0.43 and 0.98 m/s, respectively, and the bias at KEO is about 50% smaller than that at JKEO. At JKEO, the overestimation of WND and underestimation of DQ cancel and lead to a relatively small and positive bias in LHF compared to at KEO.

3.3. Comparison 4: All Heat Fluxes at the KEO

[38] Table 9 shows statistics of comparison 4. The bias in J-OFURO2 NET indicates a small overestimation, 8.6 W/m^2. The LWR, LHF, and SHF are major sources of the bias in NET, and their biases are 7.1, 5.3, and −4.1 W/m^2, respectively. As expected from the results of comparisons 1 and 2, there are some differences in biases between winter and summer. Although the NET bias in winter is quite small (2.3 W/m^2), the NET bias in summer is somewhat large (13.4 W/m^2). The biases of LHF and LWR in summer are major source of the summer bias in NET, and 9.7 and 6.7 W/m^2, respectively. The overestimation of LHF in summer is mainly due to overestimation of DQ, as described in section 3.1. The overestimation of LWR in summer is due to underestimation of downward component of LWR in ISCCP.

[39] The RMS error in NET is 56.8 W/m^2. The LHF and SWR are the largest contributions to the RMS error in NET. The RMS error in LHF and SWR are 39.7 and 34.0 W/m^2, respectively. The RMSs in NET are large in both winter and summer (>50 W/m^2), although the source of errors is different. In winter, LHF is the largest source of error and its RMS is 51.2 W/m^2. In summer, both SWR and LHF are major error sources and their RMSs are 40.4 and 31.3 W/m^2, repectively.

3.4. Comparison 5: Intercomparison

[40] The cross-comparison with the other global products (comparison 5) is limited to the period from 16 June 2004 to 9 November 2005 because of common data availability of each product. The cross-comparison of statistics for comparison 5 (Table 10) indicates that J-OFURO2 LHF is fairly accurate compared with other available global products. Although the small J-OFURO2 LHF bias is due to seasonal biases which underestimates LHF in winter season (−4.2 W/m^2) and overestimates LHF in summer season (10.3 W/m^2), these seasonal biases are fairly small compared with other global products.

[41] On the other hand, other products, especially NRA1/2 suffer from very large biases. Another satellite-derived product HOAPS3 is much better than NRA1/2. It is, however, characterized by significant seasonal biases. For instance, the bias in HOAPS3 LHF in winter is negative (−12.4 W/m^2), i.e., an underestimation, indicating that too little heat is lost by the ocean. On the other hand, the bias in summer indicates positive (28.0 W/m^2), i.e., overestimation. These seasonal biases cancel out and lead to a relatively small bias in the mean LHF bias (9.0 W/m^2). Although OAFlux shows a relatively small bias (15.6 W/m^2) compared to NRA1/2, it has similar characteristics to NRA1/2 with large positive bias in both winter and summer. OAFlux, however, has the smallest RMS of all the products and is smaller by several W/m^2 compared to those of J-OFURO2.

[42] In contrast to results for LHF, the total bias in SHF is quite small in each product. The sign of the SHF bias, however, is different for satellite-derived products than for the other products. Satellite-derived products show negative bias, i.e., underestimation, while the NRA1/2 and OAFlux

Table 9. Comparison 4 Results for All Fluxes at KEO[a]

	All			Winter (DJF)			Summer (JJA)		
	Bias	RMS	Correlation	Bias	RMS	Correlation	Bias	RMS	Correlation
LHF	5.3	39.7	0.92	−4.2	51.2	0.86	9.7	31.3	0.80
SHF	−4.1	10.8	0.93	−3.0	16.4	0.94	−2.7	7.7	0.64
SWR	−1.4	34.0	0.91	1.3	19.4	0.84	−3.1	40.4	0.86
USWR	−1.1	3.4	0.73	−2.8	2.4	0.79	0.5	3.3	0.80
DSWR	0.3	36.7	0.91	−4.1	21.4	0.83	3.5	43.3	0.86
LWR	7.1	13.4	0.83	7.6	12.6	0.80	6.7	13.8	0.73
ULWR	1.7	3.0	0.99	3.3	1.9	0.98	0.7	3.2	0.96
DLWR	−5.5	13.7	0.92	−3.9	13.2	0.84	−6.0	14.2	0.66
NET	8.6	56.8	0.95	2.3	62.3	0.91	13.4	52.8	0.80

[a]See Tables 3 and 5. Net short-wave (SWR = USWR − DSWR), net longwave (LWR = ULWR − DLWR), their upward and downward components (USWR, ULWR, DSWR, and DLWR), and the net heat flux (NET = SWR + LWR + LHF + SHF) all have units of W/m^2.

Table 10. Comparison 5 Results for Global Flux Products and KEO Buoy[a]

		All			Winter (DJF)			Summer (JJA)		
Flux	Global Product Name	Bias	RMS	Correlation	Bias	RMS	Corr.	Bias	RMS	Correlation
LHF	J-OFURO2	3.1	40.4	0.92	−4.2	51.2	0.86	10.3	30.4	0.76
	HOAPS3	9.0	48.5	0.88	−12.4	54.4	0.84	28.0	38.2	0.69
	NRA1	26.4	47.0	0.91	36.1	48.4	0.90	29.4	45.2	0.63
	NRA2	43.8	58.5	0.91	80.9	65.6	0.90	39.1	52.5	0.60
	OAFlux	15.6	36.9	0.94	35.5	47.7	0.89	16.7	28.9	0.72
SHF	J-OFURO2	−3.9	11.0	0.94	−3.0	16.4	0.94	−2.5	7.2	0.68
	HOAPS3	−2.3	16.0	0.86	−14.4	25.0	0.77	−0.3	7.6	0.61
	NRA1	3.9	16.6	0.93	16.5	21.5	0.93	−3.2	10.2	0.73
	NRA2	1.9	19.5	0.93	19.8	25.8	0.94	−5.6	11.5	0.76
	OAFlux	3.1	12.6	0.95	14.2	18.3	0.93	−3.2	6.6	0.70

[a]See Tables 3 and 5.

show positive bias, i.e., overestimation. These differences are mainly due to biases in winter, when NRA1/2 and OAFlux overestimate SHF by about 14–20 W/m^2, and satellite products show negative biases. In particular, J-OFURO2 SHF shows quite small bias in winter, −3.0 W/m^2. The RMS for SHF is also small for both OAFlux and J-OFURO2 compared with other products.

4. Summary and Discussions

[43] The new version of J-OFURO surface turbulent and net heat flux data set (J-OFURO2) has been constructed as a daily and a monthly mean on 1.0° spatial grids over the ice-free regions of global oceans for 1988–2007 and 1988–2006, with many improvements from J-OFURO1. The accuracy of J-OFURO2 surface heat fluxes was assessed here by comparing it with independent in situ observation data from the KEO and JKEO buoys deployed in the Kuroshio Extension region.

[44] The measurement accuracy of the KEO/JKEO buoys was assessed before comparison. Total errors for 10 min LHF for the KEO and JKEO are estimated to be ∼16 and ∼10 W/m^2, respectively. Assuming that a portion of these errors is random and can be reduced through time averaging, the total LHF error for the KEO/JKEO reduces to ∼4 W/m^2 for daily averaged fluxes.

[45] Errors in J-OFURO2 associated with using a bulk SST (Eskin), neglecting the surface currents (Erw), using daily means for bulk flux calculation (Edm), and aliasing temporal variability (Ets) are estimated. These errors are estimated to cause a total LHF (SHF) bias of 9.1 (2.9) W/m^2 and LHF (SHF) RMS of 15.6 (4.0) W/m^2. Neglecting to correct for the cool skin effect contributes the largest bias, while temporal sampling error is the largest source of RMS error in the daily mean LHF. This result highlights the necessity of using skin temperature data, including cool skin effect for better estimation of global surface heat fluxes. Similarly, because the buoy flux estimate relies upon the skin temperature model in the COARE 3.0 algorithm, improvement of this model and its generality should be considered in future studies.

[46] The J-OFURO2 and buoy comparison shows that J-OFURO2 air-sea heat fluxes are quite accurate. Although *Kubota et al.* [2008] revealed air-sea heat fluxes obtained from NWP at the KEO suffer from serious biases, we demonstrated that the satellite-derived surface heat flux product J-OFURO2 is quite accurate at the KEO/JKEO buoys. The bias in NET is estimated to be 8.6 W/m^2, which is near or within the error of the buoy reference time series. However, J-OFURO2 has seasonal biases that tend to cancel when averaged over a full year. This seasonality could be associated with the fact that the prevailing wind changes from being northerly (of continental origin) during winter, to being southerly (of maritime origin) during summer. Also, J-OFURO2 flux-related parameters WND and QA have significant biases that tend to cancel when estimating turbulent fluxes. These issues must be solved to develop better surface heat flux products.

[47] Likewise, the characteristics of the bias changed for different years (Table 6). Although the sign of bias for WND does not change from year to year, the sign and amplitude of biases for QS and QA are quite variable from year to year. These changes in the QS and QA biases cause a LHF bias range of 18 W/m^2 between 2004 and 2006. This result suggests the necessity of using longer time series of in situ observations by moored buoys, such as KEO and JKEO, for assessing the errors.

[48] From the cross-comparison results of the KEO buoy with five different global air-sea heat flux products including J-OFURO2, we demonstrated that J-OFURO2 air-sea heat fluxes performed very well when compared with the other global products. The total bias of LHF is smallest for J-OFURO2, and its seasonal biases are also smallest compared with other products. Although the OAFlux has the smallest RMS, the J-OFURO2 RMS is only several W/m^2 higher.

[49] An important aspect of our analysis is the comparison between the results of the KEO and JKEO. Although there is not significant difference in measurement error between the KEO and JKEO, the characteristics of error in J-OFURO2 are quite different between the two sites. The LHF bias at the KEO is negative (i.e., underestimate), while the bias at JKEO is positive (i.e., overestimate). This suggests the error characteristics are different depending on atmospheric and oceanic conditions. Continued buoy observations at these different locations, which have different atmospheric and oceanic conditions, are necessary to validate and develop better surface heat flux products.

[50] As mentioned above, improvement of seasonal biases in WND and QA is essential for the next generation of J-OFURO (J-OFURO3). It is likely that these errors are closely related to changes in the vertical atmospheric profiles induced by seasonal changes in the prevailing winds. Therefore, we are planning to develop a new QA

Table 11. Comparison of Surface Wind Speed from Single-Satellite and Multisatellite Products and the KEO Buoy[a]

Product	Bias	RMS	Correlation
SSMI F13	0.10	1.70	0.89
AMSR-E	−0.02	1.68	0.86
J-OFURO2	0.18	1.26	0.93

[a]Unit is m/s. SSMI F13 and AMSR-E are single-satellite products, and J-OFURO2 is a multisatellite product.

retrieving algorithm that uses vertical atmospheric profile information more effectively. The existing retrieving algorithm [*Schlussel et al.*, 1995] does not take account of the seasonal changes in the boundary layer physics. Also, our results demonstrate the effectiveness of using multisatellite data for reducing the RMS. Table 11 indicates that J-OFURO2 WND constructed by using multisatellite data shows significant improvement for RMS compared to single satellite WND data. We expect that the QA estimate in J-OFURO2, constructed by using only data from SSMIs series, would be improved by adopting multisatellite sampling using Aqua/AMSR-E, TRMM/TMI, and GCOM-W/AMSR2 that is planning to launch in 2011 and would lead to a reduction in the total RMS error of LHF.

[51] **Acknowledgments.** This research was funded by JAXA. The MGDSST data used in J-OFURO2 are constructed in JMA. Data from all DMSP/SSMIs, TRMM/TMI, and Aqua/AMSR-E are provided by Remote Sensing Systems. QuikSCAT data are also provided from JPL.

References

Bonjean, F., and G. S. E. Lagerloef (2002), Diagnostic model and analysis of the surface currents in the tropical Pacific Ocean, *J. Phys. Oceanogr.*, *32*, 2938–2954, doi:10.1175/1520-0485(2002)032<2938:DMAAOT>2.0.CO;2.

Brunke, M. A., C. W. Fairall, X. B. Zeng, L. Eymard, and J. A. Curry (2003), Which bulk aerodynamic algorithms are least problematic in computing ocean surface turbulent fluxes?, *J. Clim.*, *16*, 619–635, doi:10.1175/1520-0442(2003)016<0619:WBAAAL>2.0.CO;2.

Chelton, D. B., and F. J. Wentz (2005), Global microwave satellite observations of sea surface temperature for numerical weather prediction and climate research, *Bull. Am. Meteorol. Soc.*, *86*, 1097–1115, doi:10.1175/BAMS-86-8-1097.

Cronin, M. F., C. Meinig, C. L. Sabine, H. Ichikawa, and H. Tomita (2008), Surface mooring network in the Kuroshio Extension, *IEEE Syst. J.*, *2*, 424–430.

Curry, J. A., et al. (2004), Seaflux, *Bull. Am. Meteorol. Soc.*, *85*, 409–424, doi:10.1175/BAMS-85-3-409.

Fairall, C. W., E. F. Bradley, D. P. Rogers, J. B. Edson, and G. S. Young (1996), Bulk parameterization of air-sea fluxes for Tropical Ocean Global Atmosphere Coupled Ocean Atmosphere Response Experiment, *J. Geophys. Res.*, *101*, 3747–3764, doi:10.1029/95JC03205.

Fairall, C. W., E. F. Bradley, J. E. Hare, A. A. Grachev, and J. B. Edson (2003), Bulk parameterization of air-sea fluxes: Updates and verification for the COARE algorithm, *J. Clim.*, *16*, 571–591, doi:10.1175/1520-0442(2003)016<0571:BPOASF>2.0.CO;2.

Freitag, H. P., M. O'Haleck, G. C. Thomas, and M. J. McPhaden (2001), Calibration procedures and instrumental accuracies for ATLAS wind measurements, *NOAA Tech. Memo., OAR PMEL-119*, 20 pp., Pac. Mar. Environ. Lab., NOAA, Seattle, Washington, D. C.

Iwasaki, S., M. Kubota, and H. Tomita (2008), Inter-comparison and evaluation of global sea surface temperature products, *Int. J. Remote Sens.*, *29*, 6263–6280, doi:10.1080/01431160802175363.

Jiang, C. L., M. F. Cronin, K. A. Kelly, and L. Thompson (2005), Evaluation of a hybrid satellite- and NWP-based turbulent heat flux product using Tropical Atmosphere-Ocean (TAO) buoys, *J. Geophys. Res.*, *110*, C09007, doi:10.1029/2004JC002824.

Kalnay, E., et al. (1996), The NCEP/NCAR 40-year reanalysis project, *Bull. Am. Meteorol. Soc.*, *77*, 437–471, doi:10.1175/1520-0477(1996)077<0437:TNYRP>2.0.CO;2.

Kanamitsu, M., W. Ebisuzaki, J. Woollen, S. K. Yang, J. J. Hnilo, M. Fiorino, and G. L. Potter (2002), NCEP-DOE AMIP-II reanalysis (R-2), *Bull. Am. Meteorol. Soc.*, *83*, 1631–1643, doi:10.1175/BAMS-83-11-1631(2002)083<1631:NAR>2.3.CO;2.

Kelly, K. A., S. Dickinson, M. J. McPhaden, and G. C. Johnson (2001), Ocean currents evident in satellite wind data, *Geophys. Res. Lett.*, *28*, 2469–2472, doi:10.1029/2000GL012610.

Konda, M., N. Imasato, K. Nishi, and T. Toda (1994), Measurement of the sea surface emissivity, *J. Oceanogr.*, *50*, 17–30, doi:10.1007/BF02233853.

Kondo, J. (1975), Air-sea bulk transfer coefficients in diabatic conditions, *Boundary Layer Meteorol.*, *9*, 91–112, doi:10.1007/BF00232256.

Kubota, M., and S. Mitsumori (1997), Sensible heat flux estimated by satellite data over the North Pacific, in *Space Remote Sensing of Subtropical Oceans*, edited by C. T. Liu, pp. 127–136, Elsevier, New York.

Kubota, M., and T. Hihara (2008), Retrieval of surface air apecific humidity over the ocean using AMSR-E measurements, *Sensors*, *8*, 8016–8026, doi:10.3390/s8128016.

Kubota, M., N. Iwasaka, S. Kizu, M. Kondo, and K. Kutsuwada (2002), Japanese ocean flux data sets with use of Remote Sensing Observations (J-OFURO), *J. Oceanogr.*, *58*, 213–225, doi:10.1023/A:1015845321836.

Kubota, M., N. Iwabe, M. F. Cronin, and H. Tomita (2008), Surface heat fluxes from the NCEP/NCAR and NCEP/DOE reanalyses at the Kuroshio Extension Observatory buoy site, *J. Geophys. Res.*, *113*, C02009, doi:10.1029/2007JC004338.

Kurihara, Y., T. Sakurai, and T. Kuragano (2006), Global daily sea surface temperature analysis using data from satellite microwave radiometer, satellite infrared radiometer and in-situ observations (in Japanese), *Weather Bull.*, *73*, s1–s18.

Minobe, S., A. Kuwano-Yoshida, N. Komori, S. P. Xie, and R. J. Small (2008), Influence of the Gulf Stream on the troposphere, *Nature*, *452*, 206–251, doi:10.1038/nature06690.

Moore, G. W. K., and I. A. Renfrew (2002), An assessment of the surface turbulent heat fluxes from the NCEP-NCAR reanalysis over the western boundary currents, *J. Clim.*, *15*, 2020–2037, doi:10.1175/1520-0442(2002)015<2020:AAOTST>2.0.CO;2.

Qiu, B., S. M. Chen, and P. Hacker (2004), Synoptic-scale air-sea flux forcing in the western North Pacific: Observations and their impact on SST and the mixed layer, *J. Phys. Oceanogr.*, *34*, 2148–2159, doi:10.1175/1520-0485(2004)034<2148:SAFFIT>2.0.CO;2.

Reynolds, R. W., and T. M. Smith (1994), Improved global sea-surface temperature analyses using optimum interpolation, *J. Clim.*, *7*, 929–948, doi:10.1175/1520-0442(1994)007<0929:IGSSTA>2.0.CO;2.

Schlussel, P., L. Schanz, and G. Englisch (1995), Retrieval of latent-heat flux and longwave irradiance at the sea-surface from SSM/I and AVHRR measurements, *Adv. Space Res.*, *16*, 107–116, doi:10.1016/0273-1177(95)00389-V.

Small, R. J., S. P. deSzoeke, S. P. Xie, L. O'Neill, H. Seo, Q. Song, P. Cornillon, M. Spall, and S. Minobe (2008), Air-sea interaction over ocean fronts and eddies, *Dyn. Atmos. Oceans*, *45*, 274–319, doi:10.1016/j.dynatmoce.2008.01.001.

Sun, B. M., L. S. Yu, and R. A. Weller (2003), Comparisons of surface meteorology and turbulent heat fluxes over the Atlantic: NWP model analyses versus Moored buoy observations, *J. Clim.*, *16*, 679–695, doi:10.1175/1520-0442(2003)016<0679:COSMAT>2.0.CO;2.

Tokinaga, H., Y. Tanimoto, S. P. Xie, T. Sampe, H. Tomita, and H. Ichikawa (2009), Ocean frontal effects on the vertical development of clouds over the western North Pacific: In situ and satellite observations, *J. Clim.*, *22*, 4241–4260, doi:10.1175/2009JCLI2763.1.

Tomita, H., and M. Kubota (2006), An analysis of the accuracy of Japanese Ocean Flux data sets with use of Remote sensing Observations (J-OFURO) satellite-derived latent heat flux using moored buoy data, *J. Geophys. Res.*, *111*, C07007, doi:10.1029/2005JC003013.

Tomita, H., and M. Kubota (2010), Investigation of impact of sampling error and use of multi-satellite data on satellite-derived latent heat flux, *Int. J. Remote. Sens.*, in press.

Yu, L. S., and R. A. Weller (2007), Objectively analyzed air-sea heat fluxes for the global ice-free oceans (1981–2005), *Bull. Am. Meteorol. Soc.*, *88*, 527–539, doi:10.1175/BAMS-88-4-527.

M. F. Cronin, Pacific Marine Environmental Laboratory, NOAA, 7600 Sand Point Way NE, Seattle, WA 98115, USA.

H. Ichikawa, M. Konda, and H. Tomita, Research Institute for Global Change, Japan Agency for Marine and Earth Science Technology, Natsushima, Yokosuka 237-0061, Japan. (tomitah@jamstec.go.jp)

S. Iwasaki and M. Kubota, School of Marine Science and Technology, Tokai University, 3-20-1 Orido, Shimizu, Shizuoka 424-0902, Japan.